

RESEARCH

In-flight Scalar Calibration and Characterisation of the Swarm Magnetometry Package

Lars Tøffner-Clausen^{1*}, Vincent Lesur², Nils Olsen¹ and Christopher C. Finlay¹

*Correspondence:

lastec@space.dtu.dk

¹Division of Geomagnetism, DTU Space, Technical University of Denmark, Diplomvej, Kongens Lyngby, Denmark

Full list of author information is available at the end of the article

Abstract

We present the in-flight scalar calibration and characterisation of the *Swarm* magnetometry package consisting of the absolute scalar magnetometer (ASM), the vector magnetometer (VFM), and the spacecraft structure supporting the instruments. A significant improvement in the scalar residuals between the pairs of magnetometers is demonstrated, confirming the high performance of these instruments. The results presented here, including the characterization of a Sun-driven disturbance field, form the basis of the correction of the magnetic vector measurements from *Swarm* which is applied to the *Swarm* Level 1b magnetic data.

Keywords: Geomagnetism; Magnetometer; Instrument Calibration; Satellite; *Swarm*

1

2

1 Introduction

In November 2013 the European Space Agency (ESA) launched the three *Swarm* satellites named *Alpha*, *Bravo*, and *Charlie* with the objective to provide the best ever survey of the geomagnetic field and its temporal evolution ([Friis-Christensen et al., 2006](#)). Each spacecraft carries an Absolute Scalar Magnetometer (ASM) for measuring Earth's magnetic field intensity, a Vector Fluxgate Magnetometer (VFM) measuring the direction and strength of the magnetic field, and a three-head Star TRacker (STR) mounted close to the VFM to obtain the attitude needed to transform the vector readings to an Earth fixed coordinate frame. Time and position are provided by an on-board GPS receiver. The payload also includes instruments to measure plasma and electric field parameters as well as non-gravitational acceleration. More information on the mission status after two years in orbit can be found in [Floborghagen et al. \(2016\)](#).

16

One of the purposes of the scalar magnetometer (ASM) is to provide the necessary absolute magnetic data to calibrate the vector magnetometer (VFM). For this an approach similar to that adopted for the previous satellite missions Ørsted and CHAMP was foreseen (c.f. [Olsen et al., 2003](#); [Yin and Lühr, 2011](#)) since those missions carried equivalent instrumentation. However, soon after launch of *Swarm* it became clear that the magnetic field vector measurements on all three spacecraft were contaminated by unforeseen disturbances which could not be captured by the traditional in-flight calibration methods referred to above. Furthermore, the disturbances show systematic variation which could impact or map into scientific investigations based on *Swarm* magnetic data. The light blue symbols in Fig. 1 show

26

27 time series of the *scalar residuals*, which are the difference, $\Delta F = |\vec{B}_{\text{VFM}}| - F_{\text{ASM}}$,
 28 between the modulus of the VFM data, $|\vec{B}_{\text{VFM}}|$, and the magnetic intensity mea-
 29 surements, F_{ASM} , taken by the ASM instrument. Based on experience with Ørsted
 30 and CHAMP scalar residuals with sub-nanotesla level were expected (rms value
 31 well below 0.5 nT), while for *Swarm* the scatter of the residuals was observed to
 32 reach several nT, resulting in an rms value approaching 1 nT, but crucially show-
 33 ing a very clear Local Time dependence. A task force was therefore established to
 34 investigate and mitigate the effect.

35
 36 Detailed investigations of the scalar residuals ΔF and of the ASM and VFM
 37 measurements separately indicated that:

- 38 • the vector readings of the VFM are affected by a disturbance vector field;
- 39 • the scalar readings of the ASM are much less, if at all, affected.

40 Consequently the Task Force concluded to pursue models which assume the mag-
 41 netic disturbance to be affecting the VFM measurements only. Plotting ΔF as a
 42 function of the Sun incidence angles with respect to the spacecraft, reveals system-
 43 atic features of the disturbance, as shown in Fig. 3. At the start of section 2 we
 44 provide detailed definitions of the two Sun incidence angles α and β . This supports
 45 the hypothesis that a magnetic source in the vicinity of the VFM magnetometer,
 46 with strength and direction depending on the direction to the Sun (as seen from the
 47 spacecraft), is responsible. We refer to such a disturbance field vector, that depends
 48 on the direction to the Sun, as $\delta\vec{B}_{\text{Sun}}$.

49
 50 The purpose of this article is to document the details of in-flight calibration of the
 51 *Swarm* magnetometer package, including an empirical determination and removal
 52 of the Sun driven vector disturbance field $\delta\vec{B}_{\text{Sun}}$, based on a mitigation approach
 53 proposed by Vincent Lesur ([Lesur et al., 2015](#)).

54
 55 Section 2 describes the parameterisation of the model of the Sun-driven distur-
 56 bance – in following referred to as the *characterisation* of the disturbance field
 57 – and of the *calibration* of the VFM instrument, by which means determination
 58 of its intrinsic scale factors and their dependence on time and temperature, and
 59 determination of the sensor-axis non-orthogonalities. We document the adopted
 60 Iteratively Reweighted Least Squared (IRLS) estimation approach, that includes
 61 a truncated singular value decomposition (SVD) approach to solving the inverse
 62 problem. The results obtained for *Swarm Alpha*, based on data covering the pe-
 63 riod from launch (22. November 2013) until end of June 2015 (i.e. 19 months), are
 64 presented in Section 3. Application of the scheme to data from the satellites *Bravo*
 65 and *Charlie* resulted in similar levels of residual improvement and statistics, and
 66 the estimates of the Sun driven disturbance $\delta\vec{B}_{\text{Sun}}$ show generally similar behaviour
 67 and structural features as found for *Swarm Alpha*, although there are also some
 68 differences. Finally, Section 4 summarizes the findings and provides perspectives
 69 regarding further improvements of the method.

71 2 Characterisation and Calibration with Scalar Residuals

72 The Sun incidence angles α and β are crucial in our approach to *characterise* the
 73 scalar residual. To clarify, in Fig. 2 we illustrate the definition of these angles with
 74 respect to the spacecraft and the Sun position. α is the azimuth in the spacecraft
 75 x-z plane (nominally the orbit plane) and β is the “elevation” out of the x-z plane
 76 positive towards *left* (looking in the nominal flight direction; i.e. positive *opposite*
 77 the spacecraft *y* axis). Examples of values for α and β for particular Sun positions
 78 are:

- 79 • $\beta = +90^\circ$: Sun directly from $-y$ (i.e. from the left during nominal flight)
- 80 • $\beta = -90^\circ$: Sun directly from $+y$ (i.e. from the right)
- 81 • $\beta = 0^\circ, \alpha = 0^\circ$: Sun directly from $+x$ (i.e. from the front)
- 82 • $\beta = 0^\circ, \alpha = +90^\circ$: Sun directly from $-z$ (above)
- 83 • $\beta = 0^\circ, \alpha = +180^\circ$: Sun directly from $-x$ (i.e. from the back – slightly above
 84 the boom)

85 Considering how these angles vary over orbits of the *Swarm* spacecraft during nom-
 86 inal flight, we find that α varies rapidly: from 360° down to 0° within one orbit (i.e.
 87 within ≈ 90 minutes) while β , varies slowly up and down typically by $\approx 1.25^\circ$ in
 88 one day (for *Alpha* and *Charlie*, 1.20° for *Bravo*).

89
 90 Although the observed scalar residuals clearly vary with the Sun incidence angles
 91 α and β (see Fig. 3) there is no direct mapping of ΔF in terms of these parameters.
 92 This is a consequence of the scalar residuals $\Delta F \approx \delta \vec{B}_{\text{Sun}} \cdot \vec{b}_0$ being the projection
 93 of the magnetic disturbance vector $\delta \vec{B}_{\text{Sun}}$, onto the unit vector \vec{b}_0 of the ambient
 94 magnetic field direction (Earth’s main field). The former is oriented relative to
 95 the spacecraft while the latter is oriented relative to Earth, which results in the
 96 variations with the spacecraft local time (captured by β) as seen in Fig. 3. The
 97 spacecraft local time changes by 12 hours (corresponding to a change in β by 180°)
 98 within approximately $4\frac{1}{2}$ months.

99
 100 To account for the projection on to the ambient field, we consider a *vector* mag-
 101 netic disturbance $\delta \vec{B}_{\text{Sun}}(\alpha, \beta)$, with each component depending individually on the
 102 Sun incidence angles. Mathematically, we describe each component of the distur-
 103 bance field vector by a spherical harmonic expansion in α and β i.e. we consider
 104 three independent spherical harmonic expansions in all.

105
 106 This model *characterizing* the Sun-driven disturbance is co-estimated together
 107 with a model of the temporal evolution of the VFM sensitivity and an adjustment
 108 of the pre-flight estimated non-orthogonality angles of the VFM sensor. For this
 109 we perform a *scalar calibration* via a least squares fit, minimizing the discrepancy
 110 (ΔF) between the fully calibrated and corrected measurements from the ASM and
 111 the modulus of the vector measurements from the VFM after our model has been
 112 applied. Huber weights are used iteratively to eliminate the effect of anomalous
 113 measurements (“outliers”) on the estimated models.

115 2.1 Model Parameterisation

116 As outlined above, our model characterizing the Sun-driven disturbance vector
 117 $\delta\vec{B}_{\text{Sun}}$ consists of three spherical harmonic expansions up to degree and order 25,
 118 one for each of the magnetic field components in the VFM magnetometer frame,
 119 with the position of the Sun with respect to the spacecraft parameterised by the
 120 Sun incidence angles α and β . It takes the form

$$\delta\vec{B}_{\text{Sun}} = \sum_{n=0}^{25} \sum_{m=0}^n (\vec{u}_n^m \cos m\alpha + \vec{v}_n^m \sin m\alpha) P_n^m(\sin \beta)$$

121 where \vec{u}_n^m and \vec{v}_n^m are the spherical harmonic expansion coefficients, with one com-
 122 ponent for each component of the disturbance field, and P_n^m are the Schmidt semi-
 123 normalized Legendre functions. Note that $\delta\vec{B}_{\text{Sun}}$ includes static terms ($n = m = 0$),
 124 that describe a static (i.e. independent of the Sun position) disturbance vector.
 125 The disturbance field vector $\delta\vec{B}_{\text{Sun}}$ is thus described by $3 \times 26^2 = 2,028$ model
 126 coefficients.

127

128 The model for re-scaling the vector measurements and taking into account any
 129 small adjustment of the non-orthogonality of the VFM sensors, which is required in
 130 order to obtain the fully calibrated and corrected vector field measurements \vec{B}_{VFM} ,
 131 now takes the form

$$\vec{B}_{\text{VFM}} = \underline{\underline{P}}^{-1} \underline{\underline{S}}^{-1} \vec{B}_{\text{pre-flight}} - \delta\vec{B}_{\text{Sun}}$$

132 where $\vec{B}_{\text{pre-flight}}$ are the VFM measurements calibrated using the pre-flight param-
 133 eters and corrected for the pre-flight determined stray fields as described in [Tøffner-
 134 Clausen \(2015\)](#). $\underline{\underline{S}}$ is a 3×3 diagonal scaling matrix with elements

$$s_j = s^{\text{B-spline}}(t) + s_{j, T_{\text{sensor}}} T_{\text{sensor}} + s_{j, \beta} \beta$$

135 where $s^{\text{B-spline}}(t)$ is a quadratic B-spline in time with 3-month knot separation
 136 (common for all three components of the magnetic field), and $s_{j, T_{\text{sensor}}}$, $j = 1 - 3$
 137 is an adjustment of the pre-flight estimated dependency of the VFM sensitivity on
 138 its sensor temperature, T_{sensor} , for each sensor axis j . $s_{j, \beta}$ is an empirical scaling
 139 parameter and β the Sun incidence angle, as defined above. The choice of quadratic
 140 B-splines with 3-month knot separation is made to allow sufficient flexibility of the
 141 model; the exact choice of B-spline knot times is not crucial as very similar results
 142 are obtained with other, similar parameterisations. The estimated B-splines exhibit
 143 very moderate accelerations (in the case of the full model, see Fig. 6) and it may be
 144 possible to simplify the parameterisation of the time-dependence in future models,
 145 e.g. to an exponential saturation in time as this is the expected behaviour of the
 146 VFM instrument sensitivity, however an exponential model is ill-conditioned on the
 147 timespan of data used here.

148

149 $\underline{\underline{P}}$ is the non-orthogonality matrix that makes small adjustments to the pre-flight
 150 estimated non-orthogonalities of the VFM sensor (cf. [Olsen *et al.*, 2003](#))

$$\underline{\underline{P}} = \begin{pmatrix} 1 & 0 & 0 \\ -\sin u_1 & \cos u_1 & 0 \\ \sin u_2 & \sin u_3 & \sqrt{1 - \sin^2 u_2 - \sin^2 u_3} \end{pmatrix}$$

151 Our in-flight calibration model comprises 18 parameters in all; together with the
 152 2,028 parameters describing $\delta\vec{B}_{\text{Sun}}$ this results in 2,046 model parameters to be
 153 estimated, as listed in Table 1.

154 2.2 Estimation of Model Parameters: Inversion and Regularisation

155 In order to estimate the 2,046 model parameters from the scalar residuals we need
 156 to solve a nonlinear inverse problem. The nonlinearity arises from the treatment
 157 of non-orthogonalities (*Olsen et al., 2003*).

158
 159 The forward relationship between the vector of the scalar residuals, \mathbf{d} , ($d_i = \Delta F_i$,
 160 the scalar residual of the i th data point) and the model parameter vector \mathbf{m} , may
 161 therefore be written in the form

$$\mathbf{d} = \mathbf{g}(\mathbf{m}) + \mathbf{e}$$

162 where $\mathbf{g}(\mathbf{m})$ is a nonlinear function of the models parameters and \mathbf{e} is a small re-
 163 mainder, that cannot be explained by the model, which we seek to minimise.

164
 165 Linearisation of this problem is straightforward. A *regularized, iteratively-*
 166 *reweighted, least squares solution* to the inverse problem, is then obtained using
 167 the algorithm

$$\mathbf{m}_{k+1} = \mathbf{m}_k + (\underline{\underline{\mathbf{G}}}_k^T \underline{\underline{\mathbf{W}}}_k \underline{\underline{\mathbf{G}}}_k + \lambda \underline{\underline{\mathbf{R}}})^{-1} (\underline{\underline{\mathbf{G}}}_k^T \underline{\underline{\mathbf{W}}}_k [\mathbf{d} - \mathbf{g}(\mathbf{m})] - \lambda \underline{\underline{\mathbf{R}}}\mathbf{m}_k)$$

168 where at the k th iteration, $\underline{\underline{\mathbf{G}}}_k = \left. \frac{\partial \mathbf{g}(\mathbf{m})}{\partial \mathbf{m}} \right|_{\mathbf{m}=\mathbf{m}_k}$, is the appropriate Jacobian ma-
 169 trix, $\underline{\underline{\mathbf{R}}}$ is a regularization matrix discussed in detail below, and $\underline{\underline{\mathbf{W}}}_k$ is a (Huber)
 170 weighting matrix.

171

$\underline{\underline{\mathbf{W}}}_k$ is updated at each iteration, and consists of diagonal elements

$${}^k w_i = \min \left(1, \frac{c\sigma}{{}^k d_i} \right).$$

${}^k d_i$ is the scalar residual of the i th data point using model vector \mathbf{m}_k , and

$$\sigma = \sqrt{\frac{\sum_i ({}^{k-1} w_i {}^k d_i)^2}{\sum_i {}^{k-1} w_i^2}},$$

172 being a (robust) estimate of the standard deviation of the residuals at iteration k .
 173 We set $c = 2$, slightly higher than the value of 1.5 usually chosen, in order to ensure
 174 that the less numerous polar data are not overly downweighted in the determination

175 of the calibration parameters.

176

177 It turns out that the full set of 2,046 parameters is not needed to obtain good re-
 178 sults and low data misfit, which is confirmed by inspection of the eigenvalues of the
 179 matrix $(\underline{\mathbf{G}}_k^T \underline{\mathbf{W}}_k \underline{\mathbf{G}}_k + \lambda \underline{\mathbf{R}})$, as presented in Fig. 4 for *Swarm Alpha*. The magnitudes
 180 of the sorted eigenvalues (in order of decreasing magnitude) exhibit a distinct drop
 181 around 750-800 degrees of freedom, indicating the smaller eigenvalues contribute
 182 little to the solution. The inversion of this matrix was therefore finally performed
 183 using a truncated singular value decomposition (TSVD) procedure, retaining only
 184 750 degrees of freedom.

185

186 A regularization matrix $\underline{\mathbf{R}}$ is also included to help stabilize the inversion. This
 187 is necessary because the *Swarm* satellites operate in a tightly controlled attitude
 188 orientation which leads to a poor excitation of the VFM instrument along the axis
 189 perpendicular to the orbit plane (the East-West direction corresponding to the y -
 190 axis of the VFM sensor). Consequently, the parameters related to the y -axis are
 191 poorly determined in a scalar calibration. The regularization matrix $\underline{\mathbf{R}}$ is there-
 192 fore defined so that it acts on the parameters $s_{2,\text{Tsensor}}$, $s_{2,\beta}$, u_1 , and u_3 to force
 193 $s_{2,\text{Tsensor}} \simeq (s_{1,\text{Tsensor}} + s_{3,\text{Tsensor}}) / 2$ (to reflect the physical properties of the VFM
 194 sensor) and also to minimize the norms $s_{2,\beta}^2$ and $u_1^2 + u_3^2$. λ is chosen to be sufficiently
 195 large to effectively impose the regularisation on the estimated model. Note that no
 196 regularisation is directly imposed on $\delta \vec{B}_{\text{Sun}}$ but use of truncated SVD during the
 197 inversion automatically acts to suppresses structure in regions that are not well
 198 constrained by the input data.

199

200 The starting model for the inversions is “unity”, i.e. $\underline{P} = \underline{S} = \underline{I}$, where \underline{I} is
 201 the identity matrix, and $\vec{u}_n^m = \vec{v}_n^m = \vec{0}$. The inversions typically converge within
 202 25 iterations.

203 3 Results of Model Estimation for Swarm Alpha

204 The model described above is estimated for *Swarm Alpha* using data from the begin-
 205 ning of the mission (22 November 2013) until June 2015. Fig. 1 shows the final scalar
 206 residuals, i.e. the residuals after application of the model (after “calibration and
 207 correction”) of the VFM measurements, (in green) as a function of time together
 208 with the residuals of the un-corrected but re-scaled vector field measurements, i.e.
 209 $\vec{B}_{\text{VFM}} + \delta \vec{B}_{\text{Sun}}$, in light blue; these data illustrate what can be achieved with the
 210 traditional scalar calibration methods. Note the excellent reduction of the scalar
 211 residuals achieved by the model; the Huber weighted rms of the residuals drops
 212 from 963 pT to 168 pT. Table 2 provides the corresponding numbers for *Bravo* and
 213 *Charlie*.

214

215 Fig. 5 shows normal distribution plots for the scalar residuals. The top plot shows
 216 the distributions of all data for un-corrected (red) and fully corrected data (green)
 217 and demonstrates a transition from a non-Gaussian to Gaussian residual distri-
 218 bution when applying the model. The bottom plots show the distributions of the
 219 data split into 3-months periods, un-corrected to the left and corrected to the right.

220 These also demonstrate the elimination of systematic and non-Gaussian effects.

221

222 Table 3 lists the estimated s_{Tsensor} and s_{β} parameters, and the non-orthogonality
 223 values for all three *Swarm* satellites together with their estimated pre-flight values
 224 for the VFM instrument itself for reference. I.e. the table shows the adjustments
 225 applied in order to reduce the scalar residuals to the level indicated above.

226

227 Table 4 shows the increase in the weighted rms of the scalar residuals when omit-
 228 ting individual parts of the model – a full re-estimation of the remaining model
 229 parameters is carried out for each table entry. Particularly the omission of the non-
 230 orthogonalities drastically increases the misfit – the power (the mean-square) is
 231 more than doubled. Due to the stable attitude of the *Swarm* satellites, the small
 232 x - z non-orthogonality angle, u_2 , is equivalent to first order to a small, relative
 233 timeshift between the ASM and VFM measurements – 1 arc-second corresponds
 234 roughly to a 3 ms timeshift, and it has been discussed whether it would be more
 235 reasonable to introduce such timeshifts rather than adjusting the pre-flight esti-
 236 mated non-orthogonalities. However, the variations in the u_2 angles estimated by
 237 this model would imply time-shifts varying from -3 ms to $+13$ ms for the individual
 238 satellites which, to the authors, seems quite unlikely.

239

240 The temporal evolution of the scaling of the vector field measurements, $s^{B-spline}$,
 241 is shown in Fig. 6 for the various test models listed in Table 4. The full model,
 242 shown in red, shows a smooth behaviour in time, as expected from an instrument
 243 design perspective. The blue curve shows the model without s_{β} ; this exhibits some
 244 small oscillations, whereas the light brown (no s_{Tsensor}) and green (no $\delta\vec{B}_{\text{Sun}}$) curves
 245 show much higher level of oscillations indicating they are inadequate to capture the
 246 behaviour of the measurements. The elimination of the oscillations in the full model
 247 is a good indicator of the validity of this model. The magenta curve shows the model
 248 without non-orthogonalities; this is rather close to the curve of the full model and
 249 indicates the decoupling of the non-orthogonalities from any long-term temporal
 250 effect of the measurement disturbances and instruments.

251

252 Maps of the three components of the estimated disturbance fields from the full
 253 model as function of Sun incidence angles α (abscissa) and β (ordinate) are given
 254 in Figs. 7, 8, and 9 for *Swarm Alpha*, *Bravo*, and *Charlie* respectively. During nomi-
 255 nal flight, the Sun incidence angles traverse these plots horizontally from right
 256 to left, and move up or down in β as the orbit plane moves through local time.
 257 The Sun induced disturbance is observed to have temporal characteristics that are
 258 observed in the plots as horizontally stretched features, these are attributed to
 259 thermal capacitance: The Sun induced disturbance exhibits characteristic warm-up
 260 and cool-down effects, i.e. the disturbance increases when the spacecraft is exposed
 261 to the Sun, and decreases when the Sun exposure terminates. The time constants
 262 for these effects are up to tens of minutes (corresponding to several tens of degrees
 263 in the α angle). This effect is captured by the spherical harmonic model expansion
 264 of $\delta\vec{B}_{\text{Sun}}$ and yields the horizontally stretched features in Figs. 7-9. Note also the
 265 regions of nightside data (eclipse), the circled areas to the left of the figures, which

266 generally show less disturbance; this is not imposed by the model or any regulari-
267 sation, rather it is simply a result of the data itself, and thus another indicator of
268 the ability of the model to describe the observed disturbances. The plots also show
269 both the similarities and the differences in $\delta\vec{B}_{\text{Sun}}$ between the three satellites.
270

271 4 Conclusions

272 We have established a predominantly empirical model for the calibration and cor-
273 rection of the magnetic vector field measurements of the three *Swarm* spacecraft.
274 The model is based on detailed studies of the observed scalar residuals between the
275 measurements of the absolute scalar magnetometer, ASM, and the modulus of the
276 measurements of the vector field magnetometer, VFM. The model has proven to be
277 quite robust as more data are incorporated into the estimation of the model param-
278 eters, although the ambiguity of determining vector disturbances from a pure scalar
279 calibration affects the estimated correction vectors; these corrections do change
280 slightly (by a few tenths of a nT) as more data are added.

281
282 The estimated models reduce the scalar differences between the *Swarm* magne-
283 tometers to generally below 0.5 nT with rms values well below 200 pT for all three
284 satellites, and have been in operational use since April 2015 to produce corrected
285 *Swarm* Level 1b magnetic field vector data (as of version 0401).

286
287 Future evolutions of the model presented here are foreseen to include changing
288 the model of the temporal evolution of the VFM sensitivity from B-splines to an
289 exponentially decaying function. Analysis of $\delta\vec{B}_{\text{Sun}}$ also indicates that this vector is
290 generally confined to a few, distinct directions which may be incorporated in future
291 models. Finally, it may be possible to model the effect of the thermal capacitance
292 using appropriate temporal filter functions which would lead to a significant reduc-
293 tion of the number of parameters of the model.

294 *Data Availability*

295 The estimated disturbance vectors, $\delta\vec{B}_{\text{Sun}}$, are included in the operational Level 1b
296 magnetic *Swarm* data products as dB_Sun.

297
298
299 Uncorrected data are available at <ftp://swarm-diss.eo.esa.int/Advanced/> (login
300 required, access can be requested via <https://earth.esa.int/Swarm>).

302 **Competing interests**

303 The authors declare that they have no competing interests.

304 **Author's contributions**

305 LTC carried out the in-flight scalar calibration and characterisation, analysed the results, and led the writing of this
306 manuscript. VL proposed the model for the Sun induced vector disturbance, $\delta\vec{B}_{\text{Sun}}$, and made the first estimations
307 using this model. NiO and CF supported the entire project with many discussions, suggestions, and source code.

Acknowledgements

We would like to thank ESA for establishing and providing support to the ASM-VFM Task Force with the aim of investigating the source of the scalar residuals observed in the *Swarm* magnetic measurements, and developing a correction scheme. We would also like to thank this Task Force for its work in characterising the behaviour of the magnetic disturbance and for many fruitful discussions and inputs for this work. In particular, we would like to thank Peter Brauer from the VFM instrument team for detailed discussions on the modelling and on the characteristics of the VFM instruments. Two anonymous reviewers are thanked for their comments that helped to improve the clarity of the manuscript.

This paper is the IGP contribution XXXX.

Author details

¹Division of Geomagnetism, DTU Space, Technical University of Denmark, Diplomvej, Kongens Lyngby, Denmark

. ²National Magnetic Observatory Geomagnetism, Institut de Physique du Globe de Paris, 1 rue Jussieu, Paris,

France

.

References

Floberghagen, R., et al. (2016), The Swarm mission - an overview two years after launch, *Earth, Planets and Space*.

Friis-Christensen, E., H. Lühr, and G. Hulot (2006), *Swarm*: A constellation to study the Earth's magnetic field,

Earth, Planets and Space, 58, 351–358.

Lesur, V., M. Rother, I. Wardinski, R. Schachtschneider, M. Hamoudi, and A. Chambodut (2015), Parent magnetic

field models for the IGRF-12 GFZ-candidates, *Earth, Planets and Space*, 67(1), .

Olsen, N., et al. (2003), Calibration of the Ørsted vector magnetometer, *Earth, Planets and Space*, 55, 11–18.

Tøffner-Clausen, L. e. (2015), *Swarm* level 1b processor algorithms, *Esa doc. sw-rs-dsc-sy-0002*, National Space

Institute, DTU Space, Copenhagen.

Yin, F., and H. Lühr (2011), Recalibration of the CHAMP satellite magnetic field measurements, *Measurement*

Science and Technology, 22(5), 055,101, .

333 Figures

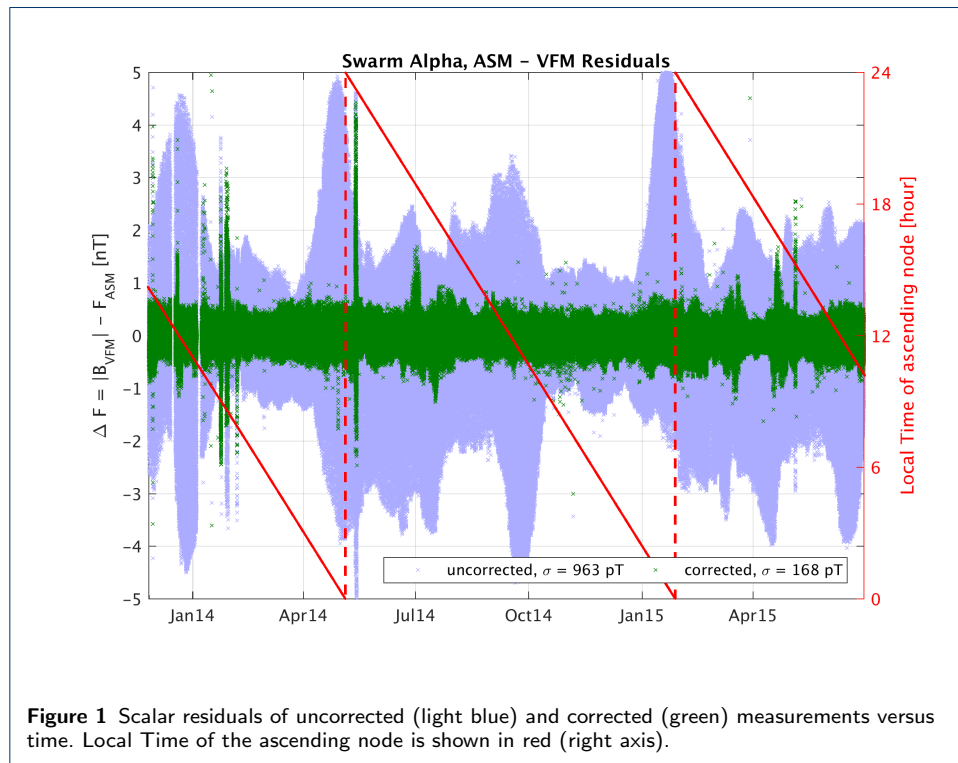


Figure 1 Scalar residuals of uncorrected (light blue) and corrected (green) measurements versus time. Local Time of the ascending node is shown in red (right axis).

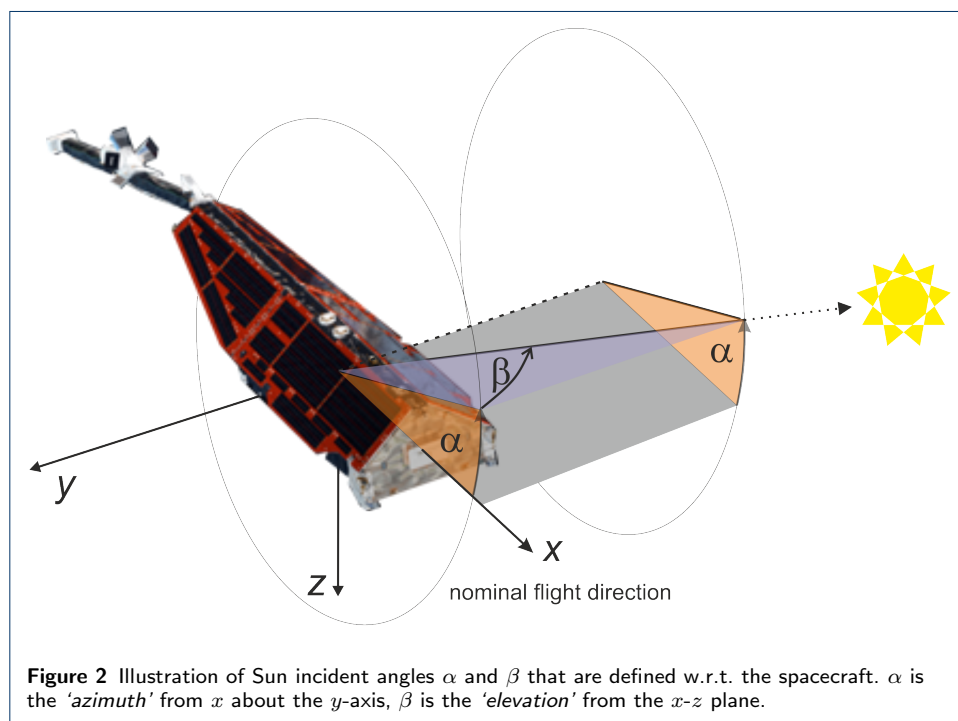
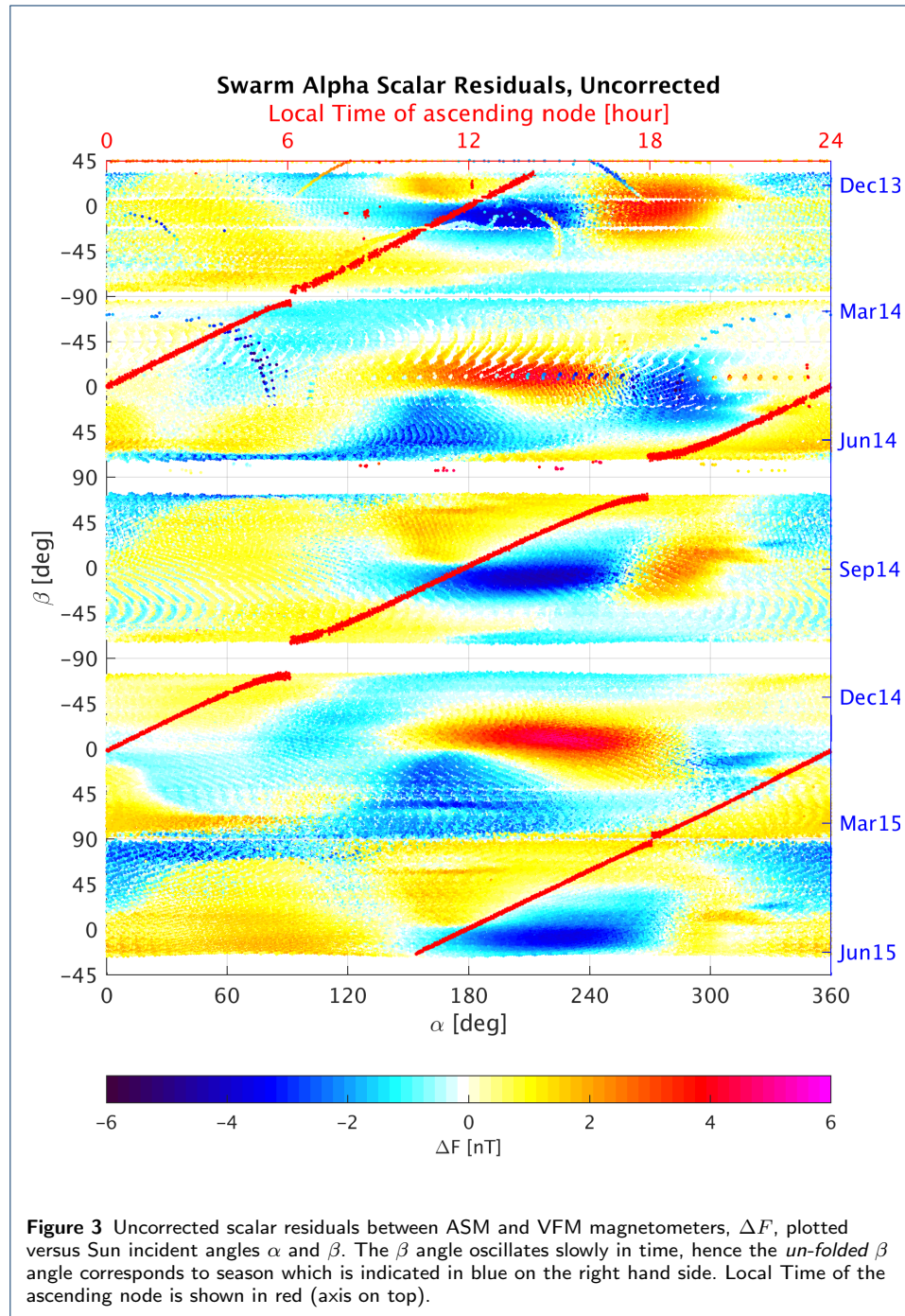
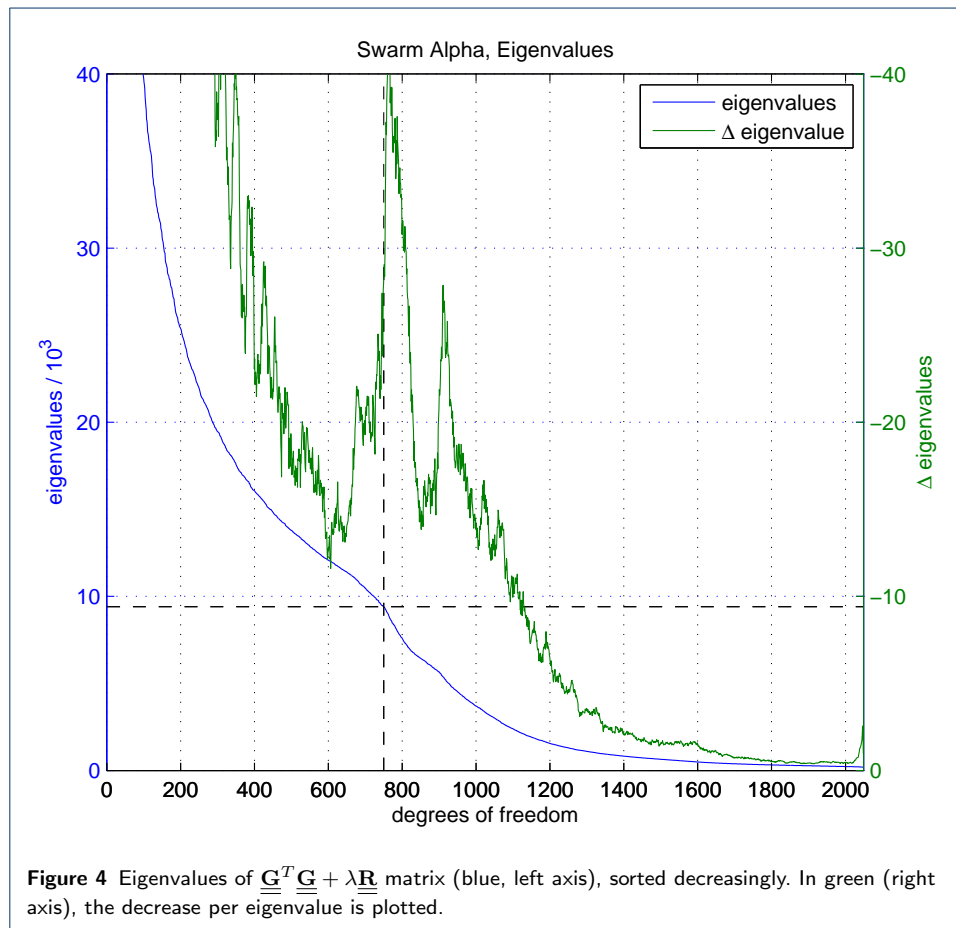
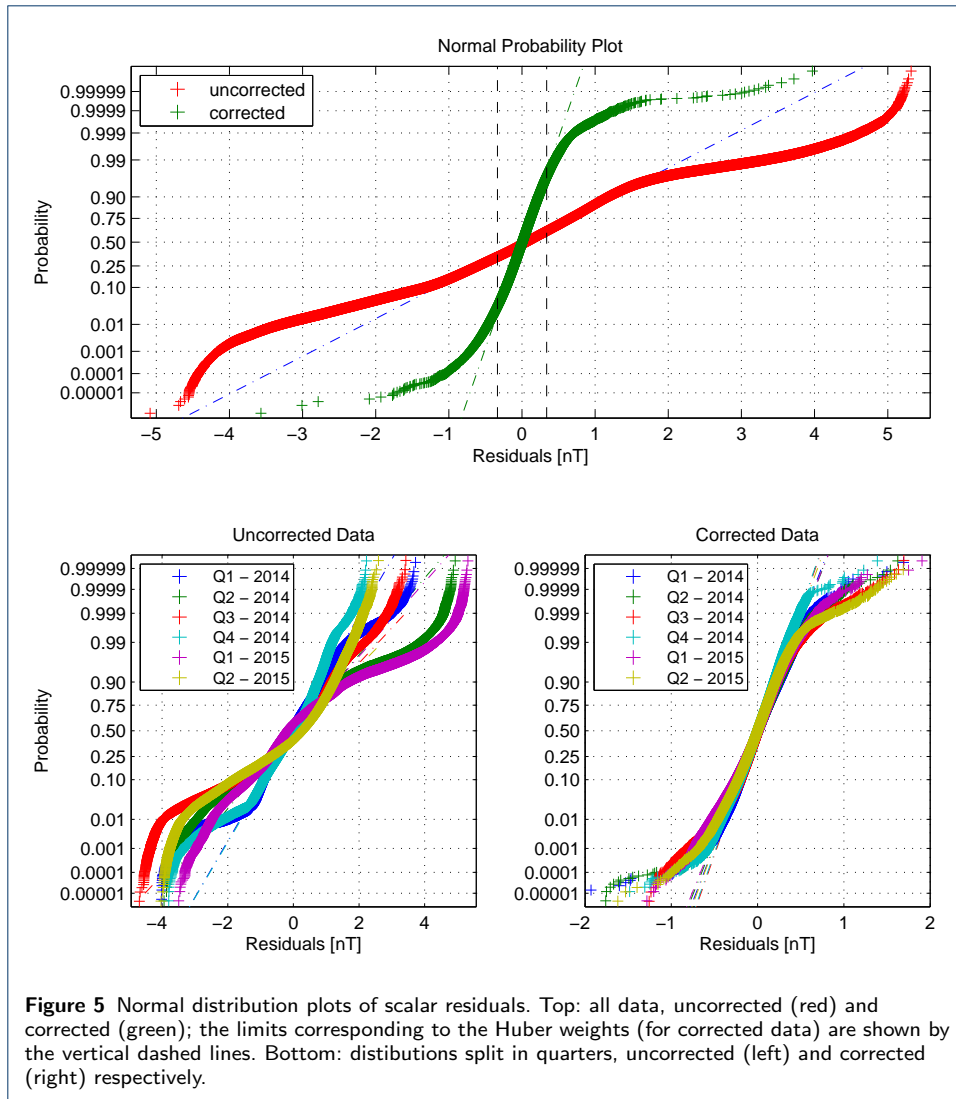
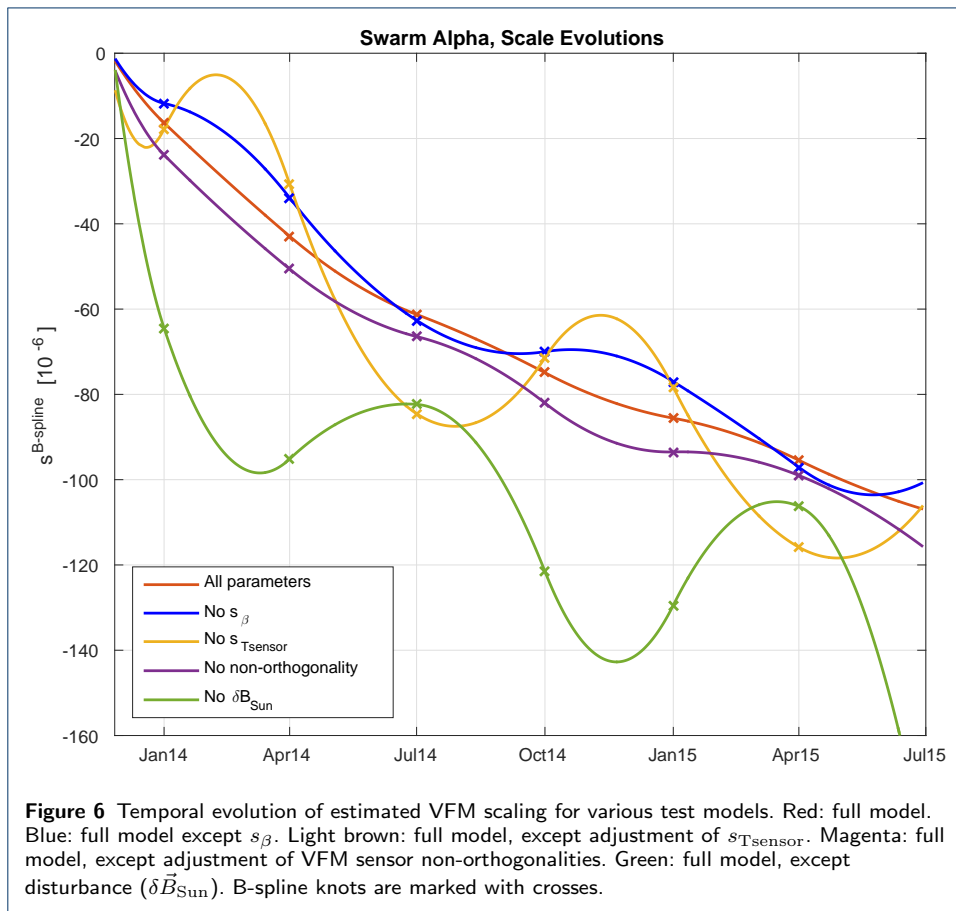


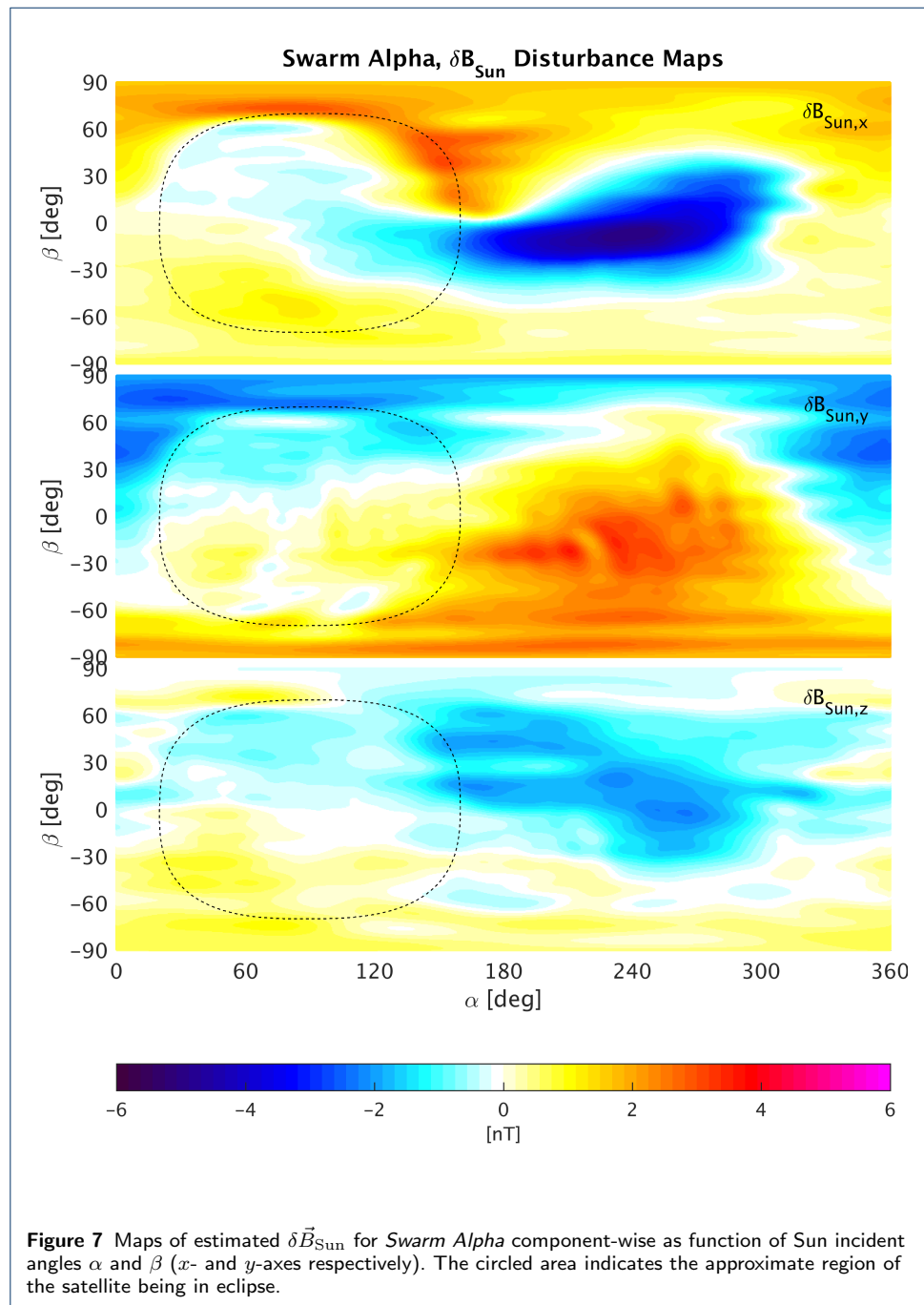
Figure 2 Illustration of Sun incident angles α and β that are defined w.r.t. the spacecraft. α is the 'azimuth' from x about the y -axis, β is the 'elevation' from the x - z plane.

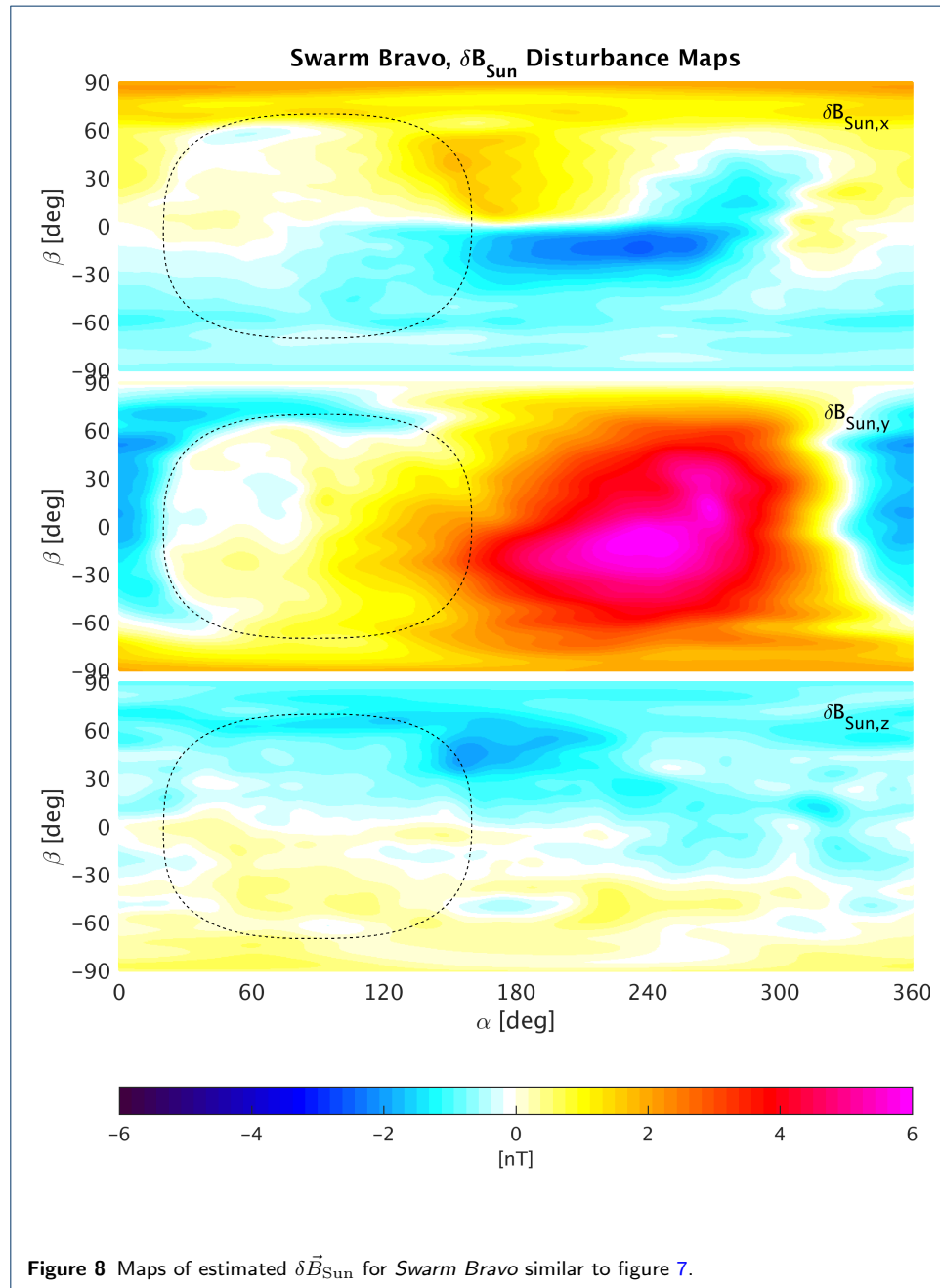


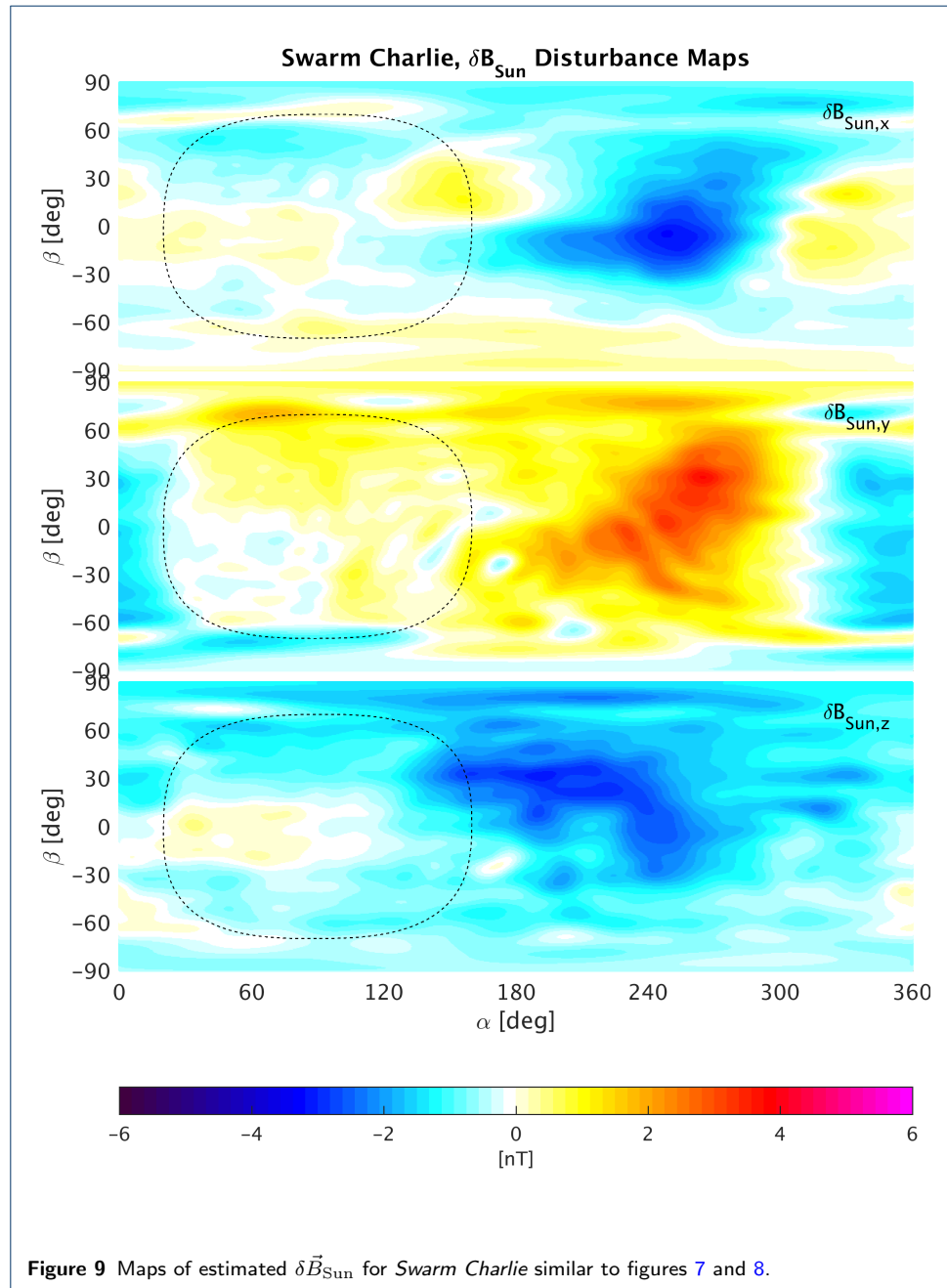












334 Tables

Table 1 Model parameters

Description	Parameters	Dimension
$\delta \vec{B}_{\text{Sun}}$	\vec{u}, \vec{v}	2,028
Sensitivity, time dependent	$s^{B\text{spline}}$	9
Sensitivity, β dependency	\vec{s}_{β}	3
Sensitivity, sensor temperature dependency	$\vec{s}_{T\text{sensor}}$	3
Non-orthogonalities	u_1, u_2, u_3	3
Total		2,046

Table 2 Scalar Residual Statistics, Uncorrected and Corrected Data.

For *Swarm Charlie* two sets of numbers are given; one set for which the ASM was still working (F_{ASM} , until 5. November 2014) and one set using the scalar data from *Swarm Alpha* mapped to the position of *Swarm Charlie* ($F_{\text{AC,map}}$). For data from 1. May 2014 through 5. November 2014 the weighted rms of $F_{\text{ASM}} - F_{\text{AC,map}}$ is 572.6 pT.

Satellite	Weighted rms [pT]	
	Uncorrected	Corrected
<i>Alpha</i>	962.6	168.3
<i>Bravo</i>	710.3	164.2
<i>Charlie</i> F_{ASM}	632.1	172.3
$F_{\text{AC,map}}$	862.1	527.7

Table 3 Estimated values for selected model parameters for all three *Swarm* satellites. The nT -equivalents of the adjustments in a 50,000 nT ambient field are: $s_{T\text{sensor}} = 10^{-6}/^{\circ}\text{C} \sim 1.25 nT$ (25°C temperature swing), $s_{\beta} = 0.1 \times 10^{-6}/\text{deg} \sim \pm 0.45 nT$ (± 90 deg), $u = 1$ arc-second $\sim 0.242 nT$.

Sat	Sensitivity/sensor temperature, $s_{T\text{sensor}}$, [$10^{-6}/^{\circ}\text{C}$]		Sensitivity/ β angle, s_{β} , [$10^{-6}/\text{deg}$]		Non-orthogonalities, $u_{1,2,3}$, [arc-seconds]	
	Pre-flight	Adjustment	Pre-flight	Adjustment	Pre-flight	Adjustment
<i>Alpha</i>	28.5	0.616	–	-0.125	102.386	-0.601
	28.8	0.780	–	0	217.403	-3.960
	28.3	0.945	–	0.012	-179.318	0.149
<i>Bravo</i>	28.3	1.168	–	-0.132	350.880	-0.558
	29.0	1.385	–	-0.003	62.432	-2.453
	28.8	1.602	–	-0.198	-147.060	1.608
<i>Charlie</i>	27.7	1.521	–	-0.090	139.140	0.094
	29.1	1.300	–	-0.038	-248.890	1.042
	28.4	1.076	–	-0.167	-109.960	0.805

Table 4 Weighted rms values for various models, *Swarm Alpha*

Model	weighted rms [pT]	Residual power (normalized)
Full model	168.3	100%
No s_{β}	176.1	107%
No $s_{T\text{sensor}}$	181.7	116%
No non-orthogonalities	250.2	221%
No $\delta \vec{B}_{\text{Sun}}$	962.6	3,269%